Exploiting Higher Order Modes for Grating Lobe Reduction in Scanning Phased Array Antennas

Zabed Iqbal, *Student Member, IEEE*, and Maria Pour, *Senior Member, IEEE*

***Abstract*—A new approach is proposed to reduce grating lobes by exciting higher order modes of conical radiation patterns in microstrip phased array antennas with a one-wavelength element spacing for medium- and wide-scan angles. The proposed concept utilizes the scanning and nulling capabilities of combined higher order modes of a circular microstrip patch as an antenna element in a seven-element hexagonal array. These elements facilitate providing suitable radiation-matched patterns for wide-scanned angles and simultaneously reducing the grating lobes for large element spacing in the order of one wavelength. In particular, for the scan angles of 35° to 75°, two higher order modes, namely the TM_{21} and TM_{31}, are excited and the grating lobes are reduced to well below -30 dB. The proposed method is also shown to be effective for near the horizon scanning with a $0.8\lambda_o$ element spacing.**

***Index Terms*— Grating lobe, phased array antenna, higher-order modes, microstrip patch.**

I. Introduction

Phased array antennas are widely used in satellite communications, radar and military applications as they have attractive features such as high gain, high tracking accuracy, swift switching capability, and electronic beam scanning. Thus, widening the beam scanning coverage has always been a hot research topic in recent years. Many methods have been reported to improve the scanning range in phased array antennas. For example, the substrate integrated waveguide (SIW) technique [1] in cavity backed microstrip arrays, the mode reconfigurable technique [2] in planar microstrip arrays, and differentially feeding technique [3] in slot antenna arrays have been developed to improve the scanning capability. Another popular method to design a wide-angle scanning phased array is to use an array element with a wide 3-dB beamwidth [4-7]. To this end, high impedance periodic structures [8-9] are often used to enhance the radiation performance of the element pattern by suppressing the surface waves and mutual coupling in the array. In general, mutual coupling in densely-packed array antennas is a real challenge. One way to mitigate this problem is to increase the separation between the array elements. However, element spacing more than half a wavelength in phased array antennas will cause grating lobes to appear in the visible region [10], which will be aggravated for wide scanning angles, leading to further reduction in the efficiency and gain of the array [11].

Many methods have been employed to address the grating lobe problem in phased array antennas. A well-known technique to decrease the grating lobes is by breaking the periodicity of the array structure in the element level [12] or the sub-array level [13-16], because the periodic nature of elements and sub-arrays generally creates grating lobes. For example, the grating lobe was reduced to -16.5 dB at the 23° scan angle in the aperiodic array in [16] by rotating and displacing periodic sub-arrays. Another virtual filling method was reported in [17], where the realization of a contiguous array was synthesized by physically separated sub-arrays with reduced grating lobes. Other recent techniques of grating lobe reduction in phased array antennas include rotation of phased array stations in square kilometer arrays [18], the use of discrete dipole elements in linear arrays [19], the ridge gap waveguide technology [20], and corrugated surface to re-radiate a portion of surface waves [21] in slot array antennas. Most of the reported approaches, however, require either complex geometry or a large number of elements to effectively reduce the grating lobes.

In this communication, a novel method is proposed to reduce grating lobes by exciting two higher order modes of conical radiation patterns in circular microstrip patch phased array antennas with large element spacing of one wavelength in the free space (λ_o) for wide scanning angles up to 75°. A dual-mode circular microstrip patch antenna operating at the TM_{21} and TM_{31} modes is used as an element to form a seven-element hexagonal phased array with one central element and six peripheral elements equally distributed over a circle of radius λ_o. Results for the broadside and medium-scan angles with the dominant TM_{11} mode and the higher order TM_{21} mode excitation were reported in a recently published paper [22] by the authors. Herein, the grating lobe reduction is further investigated for wider scan angles as well as near the horizon by simultaneously exciting two higher order TM_{21} and TM_{31} modes. The potential of the aforementioned two different dual-mode elements to reduce grating lobes in terms of scanning coverage is illustrated in Fig. 1. The corresponding results for different scan angles along with the antenna element and array formulation will be presented.

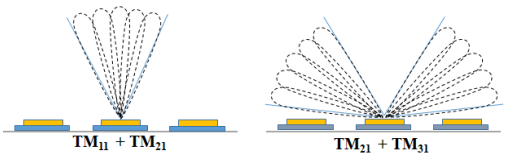

(a) (b)

Fig. 1. Scan coverage of dual-mode antenna elements in scanning arrays with large element spacing and reduced grating lobes using (a) TM_{11} and TM_{21} modes (b) proposed TM_{21} and TM_{31} modes.

II. Radiation Properties of the Proposed Element

To simultaneously widen the scanning range and mitigate the grating lobe issue in phased array antennas with large element spacing, radiation-matched elements with self-scanning and nulling capabilities are required. The potential of such elements for small- and medium-scan angles was presented by the authors in [22]. Herein, dual-mode circular microstrip patch antennas, especially those operating only at the higher order modes with conical radiation patterns, are further investigated. The modes of interest are the TM_{21} and TM_{31} modes of circular microstrip patch antennas. These modes are excited in a stacked circular patch antenna element at the frequency of 10 GHz, as depicted in Fig. 2. The top and middle patches, of radii a_2 and a_3, excite the TM_{21} and TM_{31} modes, respectively. A thin substrate with a thickness of 1.6 mm and a relative permittivity of 2.5 is used between the layers. For simplicity and without loss of generality, it is assumed that the patches are backed by an infinite ground plane, thus generating radiation patterns only into the upper hemisphere. Each patch is excited by a probe feed, placed along the x-axis. Based on the cavity model, the far-zone radiated fields of the circular microstrip patch antenna operating at the TM_{21} and TM_{31} modes can be written as [23],

Manuscript received on June xx, 2019. This work was supported in part by the National Science Foundation (NSF) CAREER Award no. ECCS-1653915.

The authors are with the Department of Electrical and Computer Engineering, The University of Alabama in Huntsville, Huntsville, AL 35899 USA (e-mail: zi0003@uah.edu ; maria.pour@uah.edu).

$$\begin{cases} E_\theta = -\frac{e^{-jk_o r}}{r}\sum_{n=2}^{3} j^n A_n F_n(\theta)\cos(n\phi) \\ E_\phi = \frac{e^{-jk_o r}}{r}\sum_{n=2}^{3} j^n A_n G_n(\theta)\sin(n\phi) \end{cases} \quad (1)$$

where,

$$\begin{cases} F_n(\theta) = J_{n-1}(k_o a_n \sin\theta) - J_{n+1}(k_o a_n \sin\theta) \\ G_n(\theta) = [J_{n-1}(k_o a_n \sin\theta) + J_{n+1}(k_o a_n \sin\theta)]\cos\theta \end{cases} \quad (2)$$

In (1), A_n is the mode content factor for the TM_{n1} mode. Mathematically, only a normalized mode content factor corresponding to the ratio of A_3/A_2, denoted herein by A_{32}, would be sufficient to define the strength of the TM_{31} mode to that of the TM_{21} mode. The A_{32} is a complex number in general to signify both the magnitude excitation ratio ($|A_{32}|$) and the phase ratio (α_{32}) between the TM_{21} and TM_{31} modes. In (2), F_n and G_n are the radiation functions governed by the Bessel function of the first kind, denoted by $J_n(x)$, and k_0 is the wave number in free space. The open-circuited edge condition of a circular microstrip patch antenna requires that the first derivative of the Bessel function $J'_n(x)$ be zero. Thus, from the zeroes of the derivative of the Bessel function, a particular radius can be calculated for each mode. The effective radii of the patches are expressed by the following equation [10],

$$a_n = \frac{\chi'_{n1}\lambda_d}{2\pi} \quad (3)$$

where λ_d is the wavelength in the dielectric substrate at the resonant frequency, and χ'_{n1} is the first zero of the derivative of the Bessel function of order n. First few zeros of $J'_n(x)$ are listed in the Table I. With the given eigenvalues of χ'_{21} = 3.0542 and χ'_{31} = 4.2012, the effective radii of patches for the TM_{21} and TM_{31} modes will become $a_2 = 0.49\lambda_d$ and $a_3 = 0.67\lambda_d$, respectively.

TABLE I
FIRST ZEROS OF THE DERIVATIVES OF BESSEL FUNCTION ($J_n'(x)$)

	TM_{11}	TM_{21}	TM_{31}
χ'_{n1}	1.8412	3.0542	4.2012

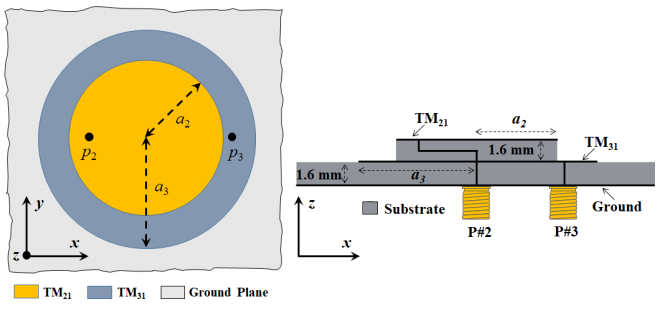

(a) (b)

Fig. 2. (a) Top view (b) cross-section view of the proposed circular microstrip patch antenna operating at the TM_{21} and TM_{31} modes with patch radii a_2 and a_3, and probe locations p_2 and p_3, respectively.

It is well established that the fundamental TM_{11} mode of the circular microstrip patch antenna only generates a broadside radiation pattern, whereas the higher order TM_{n1} modes with n>1 produce conical radiation patterns [24]. For the modes of interest in this study, i.e. TM_{21} and TM_{31} modes, their individual radiation patterns are shown in Fig. 3. As expected, both modes have conical patterns with a null at the boresight direction of $\theta = 0°$. The peaks of the normalized radiation patterns of the TM_{21} and TM_{31} modes are located around $\theta = \pm 44°$ and $\theta = \pm 56°$, respectively.

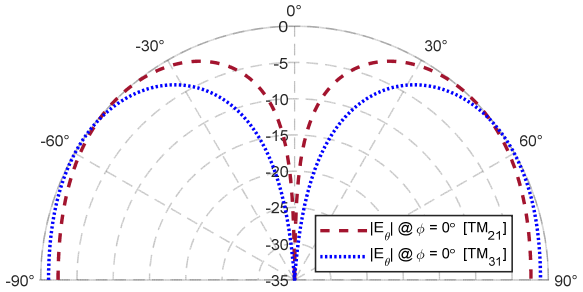

Fig. 3. Normalized radiation patterns of the TM_{21} and TM_{31} modes in a circular microstrip patch antenna.

As per (1) and (2), if one applies quadrature phase shifts of $\alpha_{32} = \pm 90°$ between the TM_{21} and TM_{31} modes, not only is the element pattern scanned, it also generates additional nulls, thus further facilitating the reduction of grating lobes in the array configuration, especially for wide scan angles. To demonstrate these nulling and self-scanning capabilities of the proposed dual-mode antenna, some representative element patterns are plotted in Fig. 4 for different values of $|A_{32}|$, when $\alpha_{32} = +90°$. As can be seen, the split beams of the individual modes shown in Fig. 3 are now effectively transformed into a single scanned beam at $\theta = +52°$, making it a suitable radiation-matched element for wide scan coverage. More interestingly, two nulls, one of which is steerable, are formed in the element patterns, which can be used to partially nullify the unwanted grating lobes. As a result, the proposed TM_{21}-TM_{31} antenna element significantly bolsters the scanning capabilities of the array, compared with the TM_{11}-TM_{21} patch elements in [22], whose element self-scanning capability was limited up to 28°, containing only a single null. It is worth mentioning that the main beam scans towards the $+xz$ and $-xz$ planes, when the phase shift α_{32} equals +90° and -90°, respectively. For brevity, the results for the former case are shown in Fig. 4.

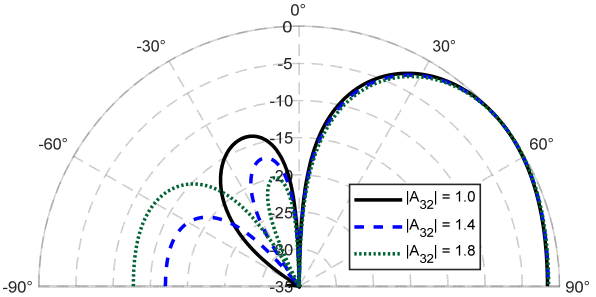

Fig. 4. Normalized radiation patterns of E_θ of the circular patch with combined TM_{21} and TM_{31} modes at the $\phi = 0°$ plane for different $|A_{32}|$, when $\alpha_{32} = +90°$.

III. FORMULATION OF THE ARRAY

The planar phased array under study is a seven-element hexagonal array placed in the xy plane, consisting of one element at the center of a circle of radius d and six peripheral elements equally spaced around the circumference of the circle with a 60° angular separation. The geometry of the array is shown in Fig. 5 and the array factor is given by,

$$AF(\theta,\phi) = 1 + w\sum_{n=1}^{6} e^{jkd\left(\sin\theta\cos\left(\phi-\frac{\pi n}{3}\right)-\sin\theta_0\cos\left(\phi_0-\frac{\pi n}{3}\right)\right)} \quad (4)$$

where the angles of the scanned beam are denoted by θ_o and ϕ_o; w is the amplitude tapering for the six peripheral elements, which is

normalized with respect to the central element. The total radiation pattern will be the product of the array factor and the element pattern defined by (4) and (1) - (2), respectively.

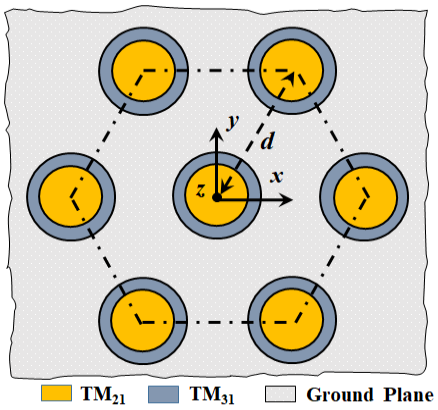

Fig. 5. Top view of the hexagonal seven-element antenna array over an infinite ground plane with six elements placed along a circle and one element in the center with element spacing *d*.

IV. Results: Total Radiation Patterns

As shown in [22] by the authors, the combined TM_{11} and higher order TM_{21} modes were needed to reduce the grating lobes for small- and medium-scan angles, when $d = \lambda_o$. To keep on reducing the grating lobes with such large element spacing, while widening the scan coverage beyond 35° scan angle, one may utilize the TM_{21} and TM_{31} modes of only conical patterns, leading to a much better radiation-matched element, which contains two nulls with enhanced self-scanning capabilities. Thus, by properly steering the position of the null to that of the grating lobe, one may partially nullify the grating lobes. In this section, we present the radiation characteristics of the seven-element planar phased array in Fig. 5 using the proposed dual-mode circular patch antenna elements for the wide scan angles. This section is arranged as follows. Section IV-A summarizes the results for wide scan angles up to 75° and large element spacing of one wavelength, which is the core finding of this paper. In Section IV-B, the technique is further expanded for near the horizon scanning with element spacing of $0.8\lambda_o$ and $0.9\lambda_o$.

A. Scan angles from 35° to 75° with $d = \lambda_o$

As the main beam of the array is further scanned towards the end-fire direction, an appropriate element pattern, such as the proposed higher-order element, with enhanced self-scanning and null steering capabilities is accordingly required. For a given scan angle, the controlling factors to reduce the grating lobes are the mode content factor of the element and the amplitude tapering coefficient of the peripheral element of the array. The former is controlled at the element level by A_{32}, whose phase shift should be 90°, as discussed in Section II. The latter, on the other hand, is determined at the array level by the coefficient w. Therefore, the critical controlling factors are $|A_{32}|$ and w, as further detailed below.

The total radiation patterns of the hexagonal array with the proposed dual-mode elements concurrently exciting the TM_{21} and TM_{31} modes are shown in Figs. 6-9 for the scan angles of 40°, 50°, 60°, and 70°, respectively, when $d = \lambda_o$. For all the aforementioned scan angles, grating lobes are reduced to below -30 dB with the proposed dual-mode elements, whose peripheral elements are properly tapered. The required mode content factor is found to be $A_{32} = 1.2\angle 90°$ for scan angles up to 75°. An extensive search routine was performed to determine the optimal amplitude distribution (w) for each scan angle. It is found that the optimal values of w for the 40° to 60° scan angles are 0.365 as shown in Fig. 6-8 and 0.375 for the scan angle of 70° as per Fig. 9. These values are close to the one reported in [22] for same element spacing of λ_o. To demonstrate the effectiveness of the method, the results in Figs. 6-9 are also compared with three other cases, namely uniform single-mode excitation, uniform dual-mode excitation, and tapered single-mode excitation. The uniform single-mode excitation serves as the reference case in this investigation, as it represents conventional phase arrays of circular patches excited at the TM_{11} mode. The grating lobes are quite large for the reference case and they tend to increase from -8.5 dB to 0 dB as the main beam is scanned from 40° to 70°. The tapered single-mode elements, on the other hand, reduce the grating lobes by about 15 dB only for the 40° scan angle, as shown in Fig. 6, and they become ineffective for wide scan angles. In contrast, the uniform dual-mode TM_{21}+TM_{31} excitation appears to be somewhat promising for scan angles up to 50°, beyond which it fails to reduce the grating lobes. Thus, as it is observed, the tapered dual-mode TM_{21}+TM_{31} excitation becomes an effective solution and a grating lobe reduction of -30 dB or lower is achieved for the scan angles as high as 75°, whose results are omitted here for brevity.

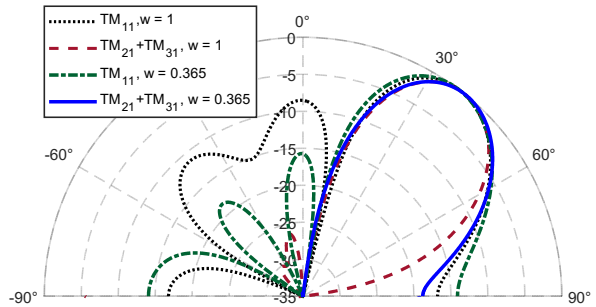

Fig. 6. Normalized radiation patterns of the seven-element phased array antenna shown in Fig. 5 with $d = \lambda_o$ and a scan angle of 40°, with both single- and dual-mode (TM_{21} and TM_{31}) antenna elements, excited by uniform and tapered amplitude distributions; for the dual-mode case, $A_{32} = 1.2\angle 90°$.

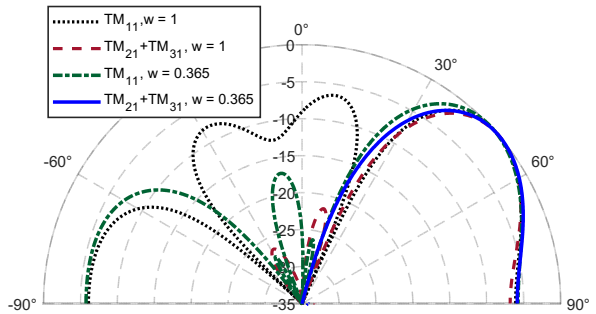

Fig. 7. Normalized radiation patterns of the seven-element phased array antenna shown in Fig. 5 with $d = \lambda_o$ and a scan angle of 50°, with both single- and dual-mode (TM_{21} and TM_{31}) antenna elements, excited by uniform and tapered amplitude distributions; for the dual-mode case, $A_{32} = 1.2\angle 90°$.

To achieve such unprecedented grating lobe reductions, the mode content factor (A_{32}) is a crucial factor because it controls the position of the steerable null as well as main-beam tilting of the element pattern. In other words, it is directly responsible for shaping the radiation-matched profile in the element level for a given scan angle by controlling the relative strength of the excited modes. The final radiation patterns for scanned main beams ranging from $\theta_o = 40°$ to $\theta_o = 70°$ of the seven-element phased array antenna with one wavelength element spacing are overlaid in Fig. 10. As shown, all the radiation patterns have reduced grating lobes below or close to -30 dB.

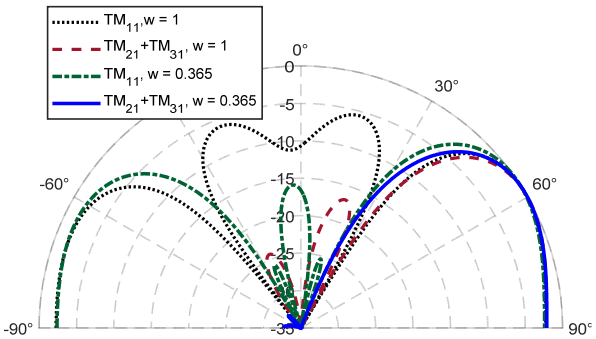

Fig. 8. Normalized radiation patterns of the seven-element phased array antenna shown in Fig. 5 with $d = \lambda_o$ and a scan angle of 60°, with both single- and dual-mode (TM_{21} and TM_{31}) antenna elements, excited by uniform and tapered amplitude distributions; for the dual-mode case, A_{32}= 1.2∠90°.

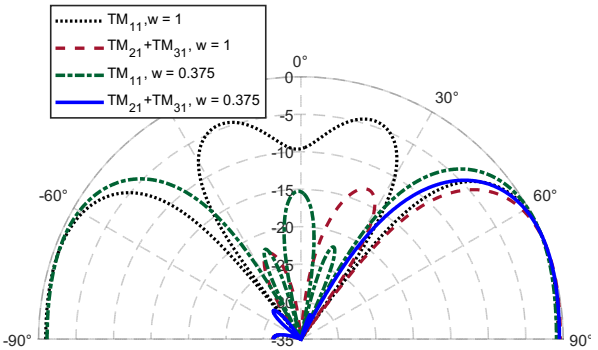

Fig. 9. Normalized radiation patterns of the seven-element phased array antenna shown in Fig. 5 with $d = \lambda_o$ and a scan angle of 70°, with both single- and dual-mode (TM_{21} and TM_{31}) antenna elements, excited by uniform and tapered amplitude distributions; for the dual-mode case, A_{32}= 1.2∠90°.

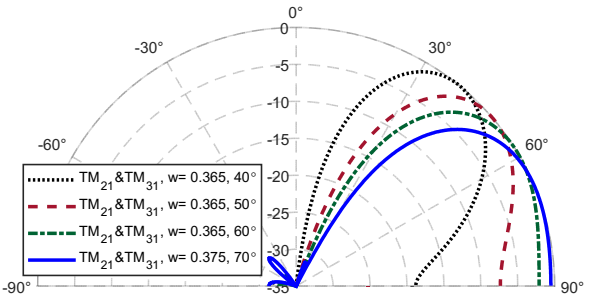

Fig. 10. Normalized radiation patterns with reduced grating lobes of the seven-element phased array antenna shown in Fig. 5 with $d = \lambda_o$, as the main beam scans from 40º to 70º.

B. Scan angles from 75° to 85° with d = 0.8λo and d = 0.9λo

In the previous subsection, the proposed hexagonal seven-element phased array antenna was analyzed and grating lobes were numerically computed by considering the element spacing as one wavelength. To extend the proposed concept of grating lobe reduction for near the horizon scanning phased array antennas, the technique is further examined for the slightly smaller element spacing of $0.9\lambda_o$ and $0.8\lambda_o$, which is shown to be promising for the wide scan angles of 80° and 85°, respectively. Both the single-mode and dual-mode excitations are investigated along with the uniform and tapered amplitude distributions. The corresponding radiation patterns are depicted in Figs. 11 and 12, for the scan angles of 80°, and 85°, respectively. For the 80° scan angle and $d = 0.9\lambda_o$, the grating lobe is reduced to -30 dB with an amplitude distribution of w = 0.360 as per Fig. 11. By further increasing the scan angle to 85° with a slightly reduced element spacing of $0.8\lambda_o$, a grating lobe reduction of -27.5 dB is realized with the proposed dual-mode TM_{21} and TM_{31} excitation when the amplitude distribution is adjusted to w = 0.365, as shown in Fig. 12.

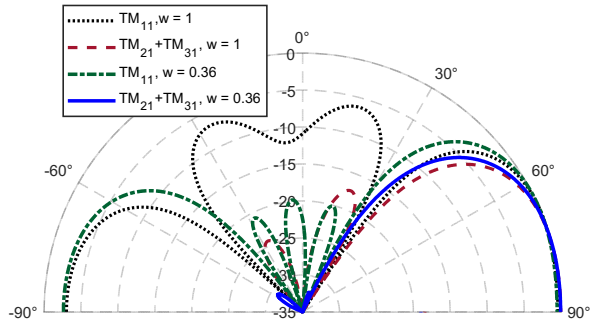

Fig. 11. Normalized radiation patterns of the seven-element phased array antenna shown in Fig. 5 with $d = 0.9\lambda_o$ and a scan angle of 80°, with both single- and dual-mode (TM_{21} and TM_{31}) antenna elements, excited by uniform and tapered amplitude distributions; for the dual-mode case, A_{32}= 1.2∠90°.

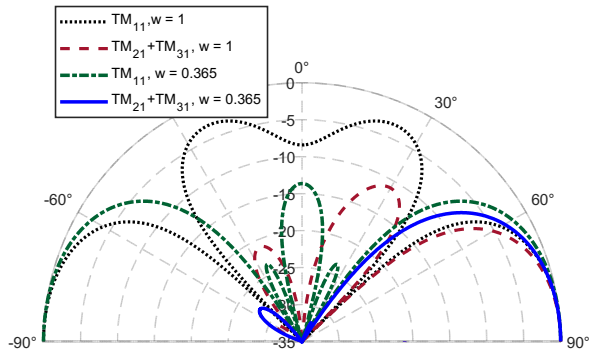

Fig. 12. Normalized radiation patterns of the seven-element phased array antenna shown in Fig. 5 with $d = 0.8\lambda_o$ and a scan angle of 85°, with both single- and dual-mode (TM_{21} and TM_{31}) antenna elements, excited by uniform and tapered amplitude distributions; for the dual-mode case, A_{32}= 1.2∠90°.

The required excitation ratios and optimized amplitude distribution of the peripheral elements for medium- and wide-scan angles are summarized in Table II.

TABLE II
FINALIZED VALUES OF THE EXCITATION RATIOS, AMPLITUDE DISTRIBUTION AND ELEMENT SPACING OF THE MATCHED ELEMENTS

Scan angle(θ_o)	Excitation Ratio ($\lvert A_{32}\rvert\angle\ \alpha_{32}$)	Amplitude Distribution (w)	Element Spacing (d)
40°	1.2∠90°	0.365	λ_o
50°	1.2∠90°	0.365	λ_o
60°	1.2∠90°	0.365	λ_o
70°	1.2∠90°	0.375	λ_o
80°	1.2∠90°	0.360	$0.9\lambda_o$
85°	1.2∠90°	0.365	$0.8\lambda_o$

V. FULL-WAVE SIMULATION RESULTS

Thus far, a circular microstrip patch antenna capable of simultaneously exciting the TM_{21} and TM_{31} modes was investiagted as a constitutive element of the proposed seven-element hexagonal phased array and both the single element and the phased array antenna were analyzed based on the cavity model in Sections II and IV, respectively, where mutual coupling and edge effects were not taken into consideration. To futher validate the analytical results and to account for the mutual coupling and edge effects in the grating lobe

reduction, full wave analyses of the phased array are performed using the finite-element based EM solver ANSYS HFSS [25]. As shown in Fig. 2, a stacked configuration of the antenna element is considered, where the top and middle patches excite the TM_{21} and TM_{31} modes, respectively, backed by an infinite ground plane in the bottom layer. Similar to the analytical study, a low permittivity substrate (Rogers Ultralam 1250) with a relative permittivity of 2.5 and a height of 1.6 mm is used as a substrate in the simulation. Fig. 13 shows the simulated scattering parameters of the dual-mode circular patch antenna, where S_{23} or S_{32} represents the mutual coupling between the TM_{21} and TM_{31} modes in a single element, and the S_{22} and S_{33} are the reflection coefficients of the ports exciting the TM_{21} and TM_{31} modes, respectively. The reference impedance for calculating the *S*-parameters is 50Ω. It is clear that the antenna element provides good impedance matching at the design frequency of 10 GHz as both S_{22} and S_{33} are well below -10 dB. It is also observed that the simulated mutual coupling, i.e., S_{23}, S_{32} between the TM_{21} and TM_{31} ports in the dual-mode antenna element is around -20 dB at the frequency of 10 GHz, which is quite low for such a stacked circular patch antenna element.

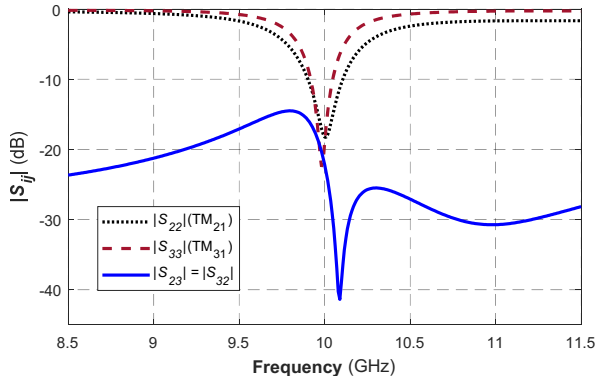

Fig. 13. Simulated magnitude of s-parameters of the dual-mode antenna element.

Having obtained the mutual coupling characteristics of the dual-mode antenna element, they are now comprehensively investigated for the proposed seven-element hexagonal phased array. Fig. 14 depicts the simulated transmission coefficients of the seven-element hexagonal array under study. There are total 14 ports in the feeding network of the phased array as 2 ports are required for each element to excite the TM_{21} and TM_{31} modes. To summarize the associated transmission coefficients, which represent mutual coupling among the array elements, three groups are defined considering (a) mutual coupling between center to edge elements, (b) mutual coupling between two adjacent edge elements and (c) mutual coupling between two non-adjacent edge elements. Each group represents mutual coupling between (i) TM_{21} to TM_{21} modes (ii) TM_{31} to TM_{31} modes, (iii) TM_{21} to TM_{31} modes and (iv) TM_{31} to TM_{21} modes, as all plotted in Fig. 14. Mutual coupling lower than -25 dB is obtained for non-adjacent elements as shown in Fig. 14(c), while mutual coupling between the center to edge elements and adjacent edge elements is around -20 dB as per Figs. 14(a) and 14(b), respectively, all of which are quite low for this array configuration.

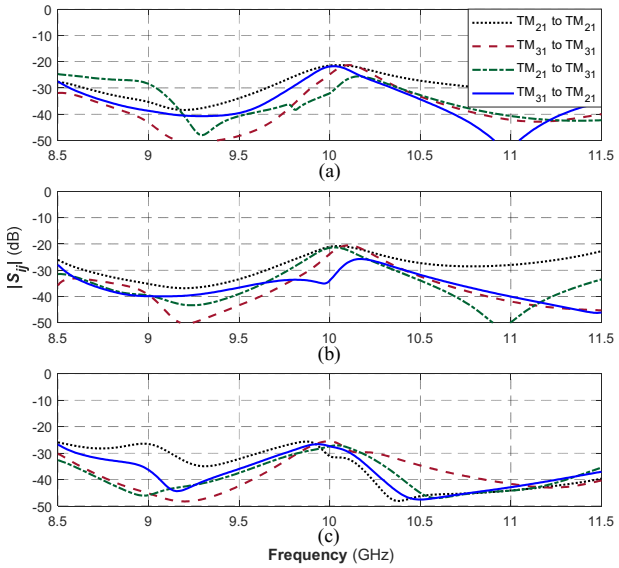

Fig. 14. Magnitude of mutual couplings between (a) center to edge and vice versa (b) edge to edge (adjacent) (c) edge to edge (non-adjacent) elements of the simulated seven-element hexagonal phased array antenna with element spacing $d = \lambda_o$.

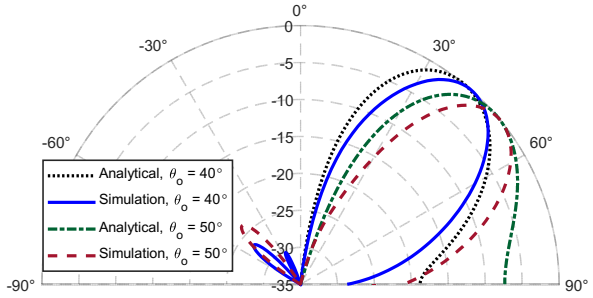

Fig. 15. Comparison of normalized radiation patterns of the seven-element hexagonal phased array using analytical approach and full wave simulation for scan angles of 40° and 50°. In both cases, element spacing $d = \lambda_o$.

A comparison between analytical and simulated radiation patterns of the seven-element hexagonal phased array is presented in Fig. 15 to further demonstrate the grating lobe reduction capability of the proposed method. Note that the mutual coupling between the array elements is now considered in the full wave EM simulation and proper phased shifts, mode content factor and amplitude distribution of the peripheral elements were applied as per our analytical prediction for different scan angles. In Fig. 15, two representative examples for the scan angles of 40° and 50° are compared with the corresponding analytical results. In simulation, the peak gain of the phased array is observed to be 18.2 dBi and 17 dBi for 40° and 50° scan angles, respectively, while the radiation efficiency is approximately 94% for the both cases. It is also seen that the simulated grating lobe levels are around -26.5 dB and -24 dB for the 40° and 50° scan angles, respectively. The discrepancy between the analytical and simulation results are mainly due to the probes and moderate mutual coupling between the adjacent elements, which were not included in the analytical study based on the cavity model.

VI. Conclusion

A novel method to reduce grating lobes in medium- to wide-scanning phased arrays, whose elements are apart by about one wavelength was proposed in this communication. The phased array was comprised of total seven elements of dual-mode circular patch

antennas, forming a hexagonal configuration. It was shown that the excitation of two higher order modes of conical radiation patterns, i.e., TM_{21} and TM_{31}, along with a tapered amplitude distribution successfully facilitated the grating lobes reduction as low as -30 dB for the scan angles up to 75° with a one-wavelength element spacing. The proposed method was further examined for near the horizon scan angles of 80° and 85°, yet again reducing the grating lobes to -27.5 dB with slightly smaller element spacing of $0.9\lambda_o$ and $0.8\lambda_o$. Finally, the full-wave simulation results were presented, which included mutual coupling among the elements, to further validate the analytical results. For such wide-scan arrays, the grating lobe reduction was realized by utilizing suitable radiation-matched elements through simultaneously exciting two higher order modes of conical patterns at the element level and a proper amplitude tapering of the array. In particular, not only did the matched element exhibit enhanced self-scanning properties, it also introduced two nulls, one of which was steerable in the vicinity of the grating lobe positions. This in turn led to the partial nullification of the unwanted grating lobes. The proposed grating lobes reduction technique has promising applications in the future generation of wide-scanning phased array antennas to be used in automotive radars, surveillance systems, multi-functional imaging radars, and many more.

REFERENCES

[1] M. H. Awida, A. H. Kamel, and A. E. Fathy, "Analysis and design of wide-scan angle wide-band phased array substrate-integrated cavity-backed patches," *IEEE Trans. Antennas Propag.*, vol. 61, no. 6, pp. 3034-3041, June 2013.

[2] X. Ding, Y.-F. Cheng, W. Shao, and B.-Z. Wang, "A wide-angle scanning phased array with microstrip patch mode reconfiguration technique," *IEEE Trans. Antennas Propag.*, vol. 65, no. 9, pp. 4548-4555, Sept. 2017.

[3] J. Guo, S. Xiao, S. Liao, B. Wang, and Q. Xue, "Dual-band and low-profile differentially fed slot antenna for wide-angle scanning phased array," *IEEE Antennas Wireless Propag. Lett.*, vol. 17, no. 2, pp. 259-262, Feb. 2018.

[4] C.-M. Liu, S. Xiao, and X.-L. Zhang, "A compact, low-profile wire antenna applied to wide-angle scanning phased array," *IEEE Antennas Wireless Propag. Lett.*, vol. 17, no. 3, pp. 389-392, Mar. 2018.

[5] Y.-F. Cheng, X. Ding, W. Shao, M.-X. Yu, and B.-Z. Wang, "2-D planar wide-angle scanning-phased array based on wide-beam elements," *IEEE Antennas Wireless Propag. Lett.*, vol. 16, pp. 876-879, Sept. 2016.

[6] G. Yang, J. Li, S. G. Zhou, and Y. Qi, "A wide-angle e-plane scanning linear array antenna with wide beam elements," *IEEE Antennas Wireless Propag. Lett.*, vol. 16, pp. 2923-2926, Sept. 2017.

[7] Y. -Q. Wen, B. -Z. Wang, and X. Ding, "Wide-beam siw-slot antenna for wide-angle scanning phased array," *IEEE Antennas Wireless Propag. Lett.*, vol. 15, pp. 1638-1641, Jan. 2016.

[8] G. Yang, J. Li, R. Xu, Y. Ma, and Y. Qi, "Improving the performance of wide-angle scanning array antenna with a high-impedance periodic structure," *IEEE Antennas Wireless Propag. Lett.*, vol. 15, pp. 1819-1822, Mar. 2016.

[9] M. Li, S. -Q. Xiao, and B. -Z. Wang, "Investigation of using high impedance surfaces for wide-angle scanning arrays," *IEEE Trans. Antennas Propag.*, vol. 63, no. 7, pp. 2895-2901, July 2015.

[10] C. A. Balanis, *Antenna Theory: Analysis and Design,* 4th ed. Wiley & Sons, Inc., Hoboken, New Jersey, USA, 2016.

[11] R. J. Mailloux, *Phased Array Antenna Handbook,* 2nd ed. Norwood, MA, USA: Artech House, 2005.

[12] B. Lu, S. X. Gong, S. Zhang, Y. Guan, and J. Ling, "Optimum spatial arrangement of array elements for suppression of grating-lobes of radar cross section," *IEEE Antennas Wireless Propag. Lett.*, vol. 9, pp. 114-117, Feb. 2010.

[13] T. J. Brockett and Y. R.-Samii, "Subarray design diagnostics for the suppression of undesirable grating lobes," *IEEE Trans. Antennas Propag.*, vol. 60, no. 3, pp. 1373-1380, Mar. 2012.

[14] P. V. Brennan, A. Narayanan, and R. Benjamin, "Grating lobe control in randomised, sparsely populated MIMO radar arrays," *IET Radar, Sonar & Nav.*, vol. 6, no. 7, pp. 587-594, Aug. 2012.

[15] D. Bianchi, S. Genovesi, and A. Monorchio, "Randomly overlapped subarrays for reduced sidelobes in angle-limited scan arrays," *IEEE Antennas Wireless Propag. Lett.*, vol. 16, pp. 1969-1972, Apr. 2017.

[16] Y. V. Krivosheev, A. V. Shishlov, and V. V. Denisenko, "Grating lobe suppression in aperiodic phased array antennas composed of periodic subarrays with large element spacing," *IEEE Antennas Propag. Magazine*, vol. 57, no. 1, pp. 76-85, Feb. 2015.

[17] B.-K. Feng and D. C. Jenn, "Grating lobe suppression for distributed digital subarrays using virtual filling," *IEEE Antennas Wireless Propag. Lett.*, vol. 12, pp. 1323-1326, Oct. 2013.

[18] J. Yu, V. A. Khlebnikov, and M. -H. Ka, "Wideband grating-lobe suppression by rotation of the phased array stations in the SKA low-frequency sparse aperture array," *IEEE Trans. Antennas Propag.*, vol. 63, no. 9, pp. 3939-3945, Sept. 2015.

[19] P. Chakravorty and D. Mandal, "Grating lobe suppression with discrete dipole element antenna arrays," *IEEE Antennas Wireless Propag. Lett.*, vol. 15, pp. 1234-1237, Nov. 2015.

[20] M. A. Sharkawy and A. A. Kishk, "Split slots array for grating lobe suppression in ridge gap guide," *IEEE Antennas Wireless Propag. Lett.*, vol. 15, pp. 946-949, Sept. 2015.

[21] C. Huang, Z. Zhao, Q. Feng, and X. Luo, "Suppression of grating lobes from a corrugated 2×2 slot antenna array with element spacing beyond a wavelength," *IET Microwave, Antennas Propag.*, vol. 5, no. 13, pp. 1607-1612, Oct. 2011.

[22] Z. Iqbal and M. Pour, "Grating lobe reduction in scanning phased array antennas with large element spacing," *IEEE Trans. Antennas Propag.*, vol. 66, no. 12, pp. 6965–6974, Dec. 2018.

[23] A. G. Derneryd, "Analysis of the microstrip disk antenna element," *IEEE Trans. Antennas Propag.*, vol. 27, no. 5, pp. 660 – 664, Sept. 1979.

[24] J. Haung, "Circularly polarized conical patterns from circular microstrip antennas," *IEEE Trans. Antennas Propag.*, vol. 32, no. 9, pp. 991-994, Sept. 1984.

[25] *High Frequency Structure Simulator (HFSS 18.0),* Canonsburg, PA, USA, ANSYS, 2018.